Environmental Science and Pollution Research (2022) 29:68636–68651
https://doi.org/10.1007/s11356-022-20698-w

RESEARCH ARTICLE

Simple preparation of a CuO@γ-Al_2O_3 Fenton-like catalyst and its photocatalytic degradation function

Gaofeng Zhu[1] · Yang Jin[1] · Mingqiao Ge[1]

Received: 19 January 2022 / Accepted: 4 May 2022 / Published online: 11 May 2022

Abstract

We designed a photocatalyst and developed sustainable wastewater purification technology, which have significant advantages in effectively solving the global problem of drinking water shortage. In this study, a new nanocomposite was reported and shown to be a catalyst with excellent performance; CuO was coated successively onto functionalized nano γ-Al_2O_3, and this novel structure could provide abundant active sites. We evaluated the performance of the CuO@γ-Al_2O_3 nanocomposite catalyst for polyvinyl alcohol (PVA) degradation under visible light irradiation. Under optimized conditions (calcination temperature, 450 °C; mass ratio of γ-Al_2O_3:$Cu(NO_3)_2{\cdot}3H_2O$, 1:15; pH value, 7; catalyst dosage, 2.6 g/L; reaction temperature, 20 °C; and H_2O_2 dosage, 0.2 g/mL), the CuO@γ-Al_2O_3 nanocomposite catalyst presented an excellent PVA removal rate of 99.21%. After ten consecutive degradation experiments, the catalyst could still maintain a PVA removal rate of 97.58%, thus demonstrating excellent reusability. This study provides an efficient and easy-to-prepare photocatalyst and proposes a mechanism for the synergistic effect of the photocatalytic reaction and the Fenton-like reaction.

Keywords CuO@γ-Al_2O_3 · Photocatalytic · Wastewater · Degradation · Fenton-like

Introduction

Due to the rapid development of industries, toxic and harmful organic pollutants are increasingly being discharged into rivers, seriously polluting the environment and endangering human health (Basheer 2018; Ali et al. 2019; Gui et al. 2019; Huang et al. 2020). In the matter of water resources, advanced oxidation processes (AOPs) are excellent methods for treating water and wastewater (Ali et al. 2020, 2021a, Ali et al. 2021b). AOPs were originally defined as treatment technologies involving the production of strong oxidants, i.e., ·OH radicals to oxidize non-biodegradable, refractory, and toxic organic pollutants under environmental conditions (Yang and Wang 2018; Smith et al. 2019; Li et al. 2019b; Ren et al. 2021). AOPs include H_2O_2/Fe^{2+} (Behnajady et al. 2007; de Luna et al. 2013), O_3/UV (Ghafoori et al. 2014), H_2O_2/UV (Dai et al. 2018), O_3/H_2O_2 (Chen et al. 2020b), and other processes (Bian et al. 2019; Agu et al. 2020; Aghayi-Anaraki and Safarifard 2020; Ren et al. 2021), which involve the generation of hydroxyl radicals (·OH) by the decomposition of the added O_3 or H_2O_2. Photocatalytic materials and photocatalytic reactions have significant application potential in the production of clean energy and efficient removal of environmental pollutants (Strieth-Kalthoff et al. 2018; Li et al. 2019a; Zhao et al. 2020; Wang et al. 2020b). Therefore, the development of a new type of catalyst with industrial value, low cost, and high efficiency is crucial (Gao et al. 2017; Ali et al. 2018; Chen et al. 2018, 2020a; Zhang et al. 2020; Basheer 2020). Since the discovery of photocatalytic water splitting by Fujishima and Honda in the early 1970s, photocatalytic processes using semiconductor materials have been regarded as promising methods because of their outstanding advantages: low cost, environmental friendliness, and sustainability.

Semiconductor photocatalysis has significant potential for reducing environmental pollution by using sunlight (Colmenares et al. 2017; Zhou et al. 2018; Wang et al. 2018). As a significant oxidation technology, photocatalytic oxidation has received considerable attention from researchers in recent years because of its advantages: photocatalytic oxidation can be carried out under mild reaction conditions, and it is a green

Responsible Editor: Guilherme L. Dotto

✉ Mingqiao Ge
7180707027@stu.jiangnan.edu.cn

[1] School of Textile Science and Engineering, Jiangnan University, Wuxi 214122, China

method; furthermore, it involves the generation of strong oxidants, and it exhibits high efficiency (Kamat 2017; Kisch 2017; Hodges et al. 2018). In recent years, many novel catalysts have been reported for the degradation of organic pollutants (Li et al. 2012, 2020b; Zhao et al. 2017; Yang and Wang 2018; Zhou et al. 2020; Dai et al. 2020; Liang et al. 2020a). However, there are still a few high-efficiency and easy-to-prepare photocatalytic materials that can be used on a large scale for the removal of environmental pollutants. Among the studied photocatalytic materials, copper oxide (CuO) is particularly important due to its availability, high chemical inertness, high photocorrosion resistance to light irradiation, and long-term stability (Ding et al. 2018; Raees et al. 2021; Islam et al. 2021). The current methods used for preparing catalysts include the impregnation-calcination method, template method, emulsion polymerization method, and self-assembly method (Xiao et al. 2019; Liang et al. 2020b). However, it is difficult to control the diameter and microstructure of microspheres; therefore, these methods have some limitations. Moreover, the prepared catalysts can easily agglomerate; this reduces the specific surface area of the catalyst, thereby affecting the catalytic performance. To solve these problems, we used spray drying and calcination methods to prepare a CuO@γ-Al_2O_3 nanocomposite catalyst having a special structure. Spray drying combined with calcination has the advantages of excellent repeatability, fast speed, and simple operation, and it is an effective method for preparing uniformly dispersed catalysts. Nano γ-Al_2O_3 exhibits high adsorption capacity and catalytic activity as well as excellent mechanical properties; moreover, it is a very suitable carrier for the active components of a catalyst (Li et al. 2020a, 2021a; Wang et al. 2021).

On the basis of the abovementioned analysis, a CuO@γ-Al_2O_3 nanocomposite catalyst was prepared by spray drying and calcination methods. Furthermore, the effects of the calcination temperature, mass ratio of γ-Al_2O_3:$Cu(NO_3)_2{\cdot}3H_2O$, pH value, catalyst dosage, H_2O_2 dosage, and dark conditions were investigated to optimize the performance of the photocatalytic Fenton-like system for the degradation of PVA, rhodamine B, and reactive red X-3B. Importantly, the synergistic effect of the photocatalytic reaction and the Fenton-like reaction and its possible mechanism were systematically explained. Therefore, this study can provide insights for constructing novel catalysts and developing an efficient electron transfer platform to accelerate the removal of environmental pollutants.

Experimental section

Materials

A PVA fabric was obtained from Baohualin Industrial Development Co. Ltd. Nano γ-Al_2O_3 (10 nm) was purchased from Beijing Enokai Technology Co. Ltd. Rhodamine B and reactive red X-3B were purchased from Jinan Haoxing Chemical Co. Ltd. Potassium iodide (KI), hydrogen peroxide (H_2O_2, 30%, in water), boric acid (H_3BO_3), iodine (I_2), concentrated nitric acid (HNO_3), and copper nitrate trihydrate ($Cu(NO_3)_2{\cdot}3H_2O$) were obtained from Sinopharm Group Chemical Reagent Co. Ltd. All the chemicals used in this research were of reagent grade, and they were used without further purification. Deionized water was used in all the experiments of this study.

Preparation of the CuO@γ-Al_2O_3 nanocomposite catalyst

The CuO@γ-Al_2O_3 nanocomposite catalyst was prepared by spray drying and calcination methods. First, nano γ-Al_2O_3 and $Cu(NO_3)_2{\cdot}3H_2O$ were weighed in proportion. Then, $Cu(NO_3)_2{\cdot}3H_2O$ was dissolved completely under stirring in 800-mL water in a 1000-mL beaker. Next, nano γ-Al_2O_3 was added, and the suspension was continuously stirred for 3 h. The concentration of the resulting nano γ-Al_2O_3 and $Cu(NO_3)_2{\cdot}3H_2O$ solution was obtained using the mass ratio of nano γ-Al_2O_3 to $Cu(NO_3)_2{\cdot}3H_2O$; for example, for 1:1, 1:5, 1:10, 1:15, and 1:20, 1, 5, 10, 15, and 20 represent the quantities of $Cu(NO_3)_2{\cdot}3H_2O$, whereas 1 corresponds to the quantity of nano γ-Al_2O_3 used for preparing the nano γ-Al_2O_3 and $Cu(NO_3)_2{\cdot}3H_2O$ solution. The CuO@γ-Al_2O_3 nanocomposite catalyst was prepared by a spray drying method by using the nano γ-Al_2O_3 and $Cu(NO_3)_2{\cdot}3H_2O$ solution as the starting material and passing it through a small spray dryer (QFN-8000S, Shanghai Guanmou Industrial Co., Ltd). The nano γ-Al_2O_3 and $Cu(NO_3)_2{\cdot}3H_2O$ solution was sprayed at 180 °C using hot air as the carrier gas. The dried CuO@γ-Al_2O_3 nanocomposite catalyst was collected by a cyclone separator. The CuO@γ-Al_2O_3 nanocomposite catalyst was easily prepared via calcining the CuO@γ-Al_2O_3 nanocomposite particles in a high-temperature furnace (GSL-1600X, Hefei Kejing Material Technology Co., Ltd) under an N_2 atmosphere. The calcination temperatures were set at 350 °C, 400 °C, 450 °C, 500 °C, 550 °C, and 600 °C in a programmable tube furnace. The calcination time was 3 h. The resulting CuO@γ-Al_2O_3 nanocomposite catalysts were named as CuO@γ-Al_2O_3(1:15)-350, CuO@γ-Al_2O_3(1:15)-400, CuO@γ-Al_2O_3(1:15)-450, CuO@γ-Al_2O_3(1:15)-500, CuO@γ-Al_2O_3(1:15)-550, CuO@γ-Al_2O_3(1:15)-600, CuO@γ-Al_2O_3(1:5)-450, CuO@γ-Al_2O_3(1:10)-450, CuO@γ-Al_2O_3(1:15)-450, and CuO@γ-Al_2O_3(1:20)-450, where 350, 400, 450, 500, 550, and 600 represent the calcination temperatures; furthermore, the ratio in the brackets refers to the mass ratio of nano γ-Al_2O_3 and $Cu(NO_3)_2{\cdot}3H_2O$ solutions, as described above.

Determination of photocatalytic reaction performance

First, an aqueous solution of the PVA fabric was prepared using deionized water (dissolution temperature: 95 °C), and the concentration of the solution was 2.5 g/L. Rhodamine B and reactive red X-3B were dissolved in deionized water via stirring in a 500-mL beaker; the concentration of all the aqueous solutions of Rhodamine B and reactive red X-3B was 200 μg/mL. All photocatalytic experiments were performed in a 500-mL glass beaker under sunlight, and the reaction temperature was room temperature (20 °C). The pH value of the reaction solution was adjusted via concentrated HNO_3 or an aqueous solution of NaOH. The photocatalytic reaction was initiated by adding an appropriate amount of the CuO@γ-Al_2O_3 nanocomposite catalyst, followed by adding H_2O_2 (30%) into the reaction solutions. Then, the optimal reaction conditions for degrading PVA were obtained via photocatalytic experiments. At last, in order to further determine the catalytic performance of the CuO@γ-Al_2O_3 nanocomposite catalyst, rhodamine B and reactive red X-3B (aqueous solutions) were used as the target pollutants. The concentrations of PVA, rhodamine B, and reactive red X-3B were measured according to the equations provided in the supplementary material (Table S1 and Fig. S1). All experiments were repeated three times, and the experimental data were recorded as the mean and standard deviation. The removal rate can be calculated using Eq. (1):

$$\text{Removal rate} = \frac{C_0 - C_t}{C_0} \times 100\% \quad (1)$$

Here, C_0 and C_t represent the concentrations of PVA, rhodamine B, and reactive red X-3B before and after degradation, respectively.

A pseudo-first-order kinetic model was used to evaluate the photocatalytic degradation curve of PVA. The reaction rate constant, k_{obs}, was calculated using Eq. (2) and Eq. (3):

$$-\frac{dC}{dt} = k_{obs} \bullet C \quad (2)$$

$$ln(\frac{C_0}{C_t}) = k_{obs} \bullet t \quad (3)$$

Here, C_0 is the initial concentration of PVA aqueous solution, and C_t is the concentration of PVA at time t.

Characterization

The morphologies and structures of CuO@γ-Al_2O_3 nanocomposite catalysts were characterized via scanning electron microscopy (SEM) with a working distance of 5 mm and at an accelerating voltage of 15 kV. The X-ray diffraction (XRD) patterns were obtained by using a D2 PHASER X-ray diffractometer (Bruker AXS GmbH, Germany); XRD was conducted at room temperature with Cu Kα radiation ($\lambda = 1.540$ Å). X-ray photoelectron spectroscopy (XPS) was conducted by using a VG ESCALAB MK II instrument, and the Al Kα X-ray radiation was 1486.6 eV. The Brunauer–Emmett–Teller–specific surface area of the CuO@γ-Al_2O_3 nanocomposite catalyst was studied using nitrogen adsorption–desorption isotherms. A UV-1800PC spectrophotometer (Shanghai Mapada Instruments Co., Ltd) was used to measure the concentrations of PVA, rhodamine B, and reactive red X-3B. The analyzed wavelengths of PVA, rhodamine B, and reactive red X-3B were 645 nm, 554 nm, and 539 nm, respectively. The total organic carbon (TOC, SHIMADZU TOC-VCPH) analysis confirmed the mineralization of polyvinyl alcohol. ICP-OES/MS (Perkin Elmer, USA) was conducted to obtain the concentration of the released metal ions. UV–vis diffuse reflectance spectroscopy (DRS) was conducted by using a UV-3600i Plus spectrophotometer.

Reusability experiments

To study the reusability of the CuO@γ-Al_2O_3 nanocomposite catalyst, the used CuO@γ-Al_2O_3 nanocomposite catalysts were recovered after PVA degradation for 120 min in the first run via centrifugation, separation, and drying with deionized water. The recovered CuO@γ-Al_2O_3 nanocomposite catalysts were reused to degrade PVA in the next run. After reaction for 120 min, the removal rate of PVA was determined by a UV-1800PC spectrophotometer. The degradation test was repeated ten times. The catalyst was characterized by XRD after 10 cycles.

Results and discussion

Characterization of the CuO@γ-Al_2O_3 nanocomposite catalyst

SEM and EDS characterization

Figure 1 shows the SEM images of CuO@γ-Al_2O_3(1:1)-450, CuO@γ-Al_2O_3(1:5)-450, CuO@γ-Al_2O_3(1:10)-450, CuO@γ-Al_2O_3(1:15)-450, and CuO@γ-Al_2O_3(1:20)-450, the elemental mapping image, and the EDS spectrum of the CuO@γ-Al_2O_3(1:15)-450 nanocomposite catalyst. The SEM images indicate the irregular structure and bulk morphology of the CuO@γ-Al_2O_3 nanocomposite catalyst, which were due to the crystallization of CuO on the surface of γ-Al_2O_3 after calcination. The particle size of the catalyst was about 5–10 μm.

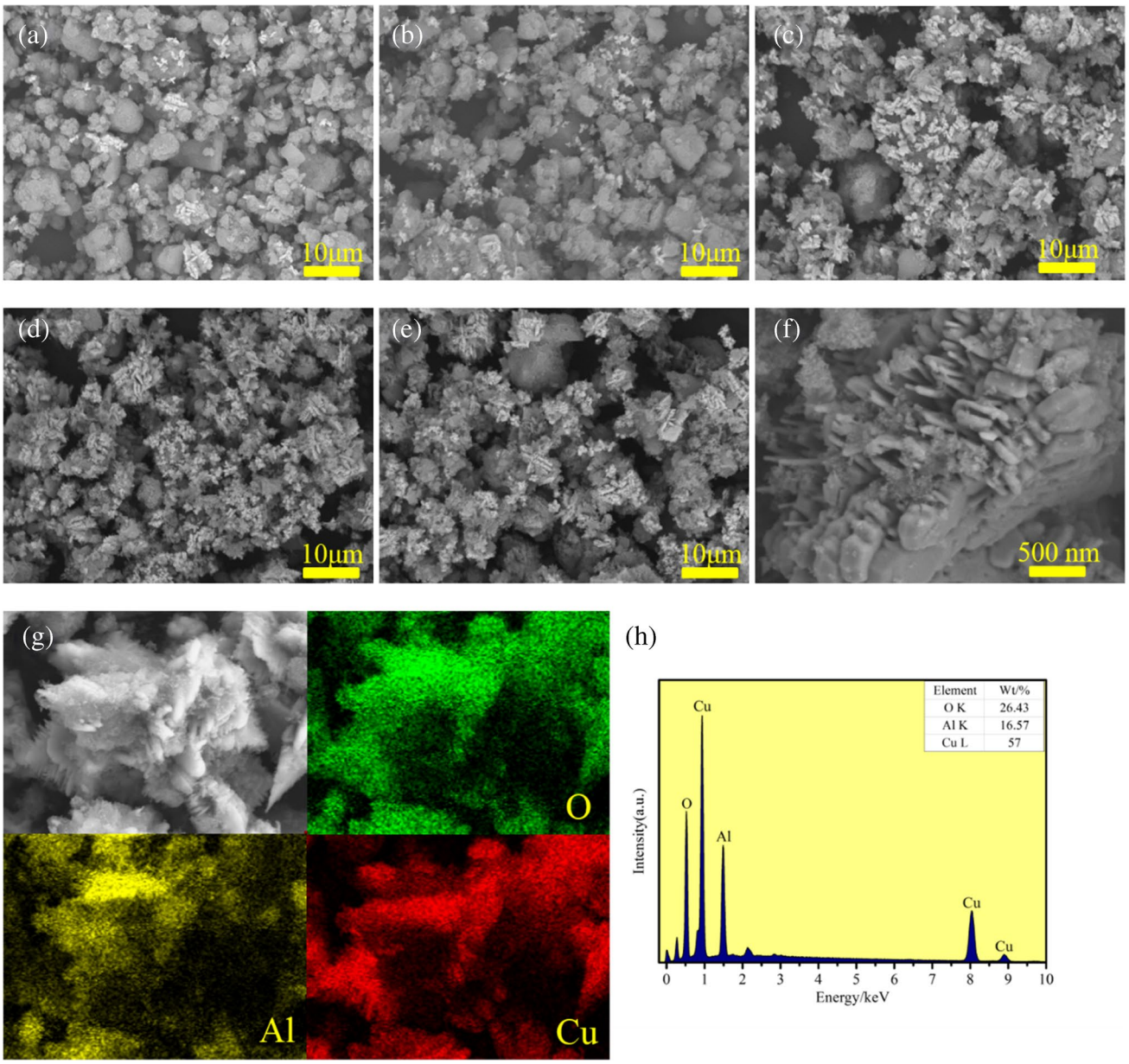

Fig. 1 The SEM images (**a**–**e**) of CuO@γ-Al2O3(1:1)-450, CuO@γ-Al2O3(1:5)-450, CuO@γ-Al2O3(1:10)-450, CuO@γ-Al2O3(1:15)-450, and CuO@γ-Al2O3(1:20)-450; enlarged image (**f**); elemental mapping image (**g**); and EDS spectrum (**h**)

In comparison, as the proportion of $Cu(NO_3)_2{\cdot}3H_2O$ increased, the number of CuO crystals on the surface of γ-Al_2O_3 also increased. Furthermore, the catalyst exhibited high dispersibility because of spray drying and calcination, and this irregular shape further increased the specific surface area. To further confirm the composition of the CuO@γ-Al_2O_3(1:15)-450 nanocomposite catalyst, EDS was conducted. The EDS spectrum is shown in Fig. 1(h); it can be observed that the atomic masses of O and Cu were 26.43% and 57%, respectively, indicating the high content of the active component CuO on γ-Al_2O_3.

XRD analysis

The crystal structures of the nanocomposite catalysts were verified by X-ray powder diffraction (XRD). Figure 2(a) shows the XRD patterns of CuO@γ-Al_2O_3(1:15)-350, CuO@γ-Al_2O_3(1:15)-400, CuO@γ-Al_2O_3(1:15)-450, CuO@γ-Al_2O_3(1:15)-500, CuO@γ-Al_2O_3(1:15)-550, and CuO@γ-Al_2O_3(1:15)-600; Fig. 2(b) exhibits the XRD patterns of CuO@γ-Al_2O_3(1:1)-450, CuO@γ-Al_2O_3(1:5)-450, CuO@γ-Al_2O_3(1:10)-450, CuO@γ-Al_2O_3(1:15)-450, and CuO@γ-Al_2O_3(1:20)-450. As shown in Fig. 2(a–b), when compared with the standard card of CuO (PDF#72–0629),

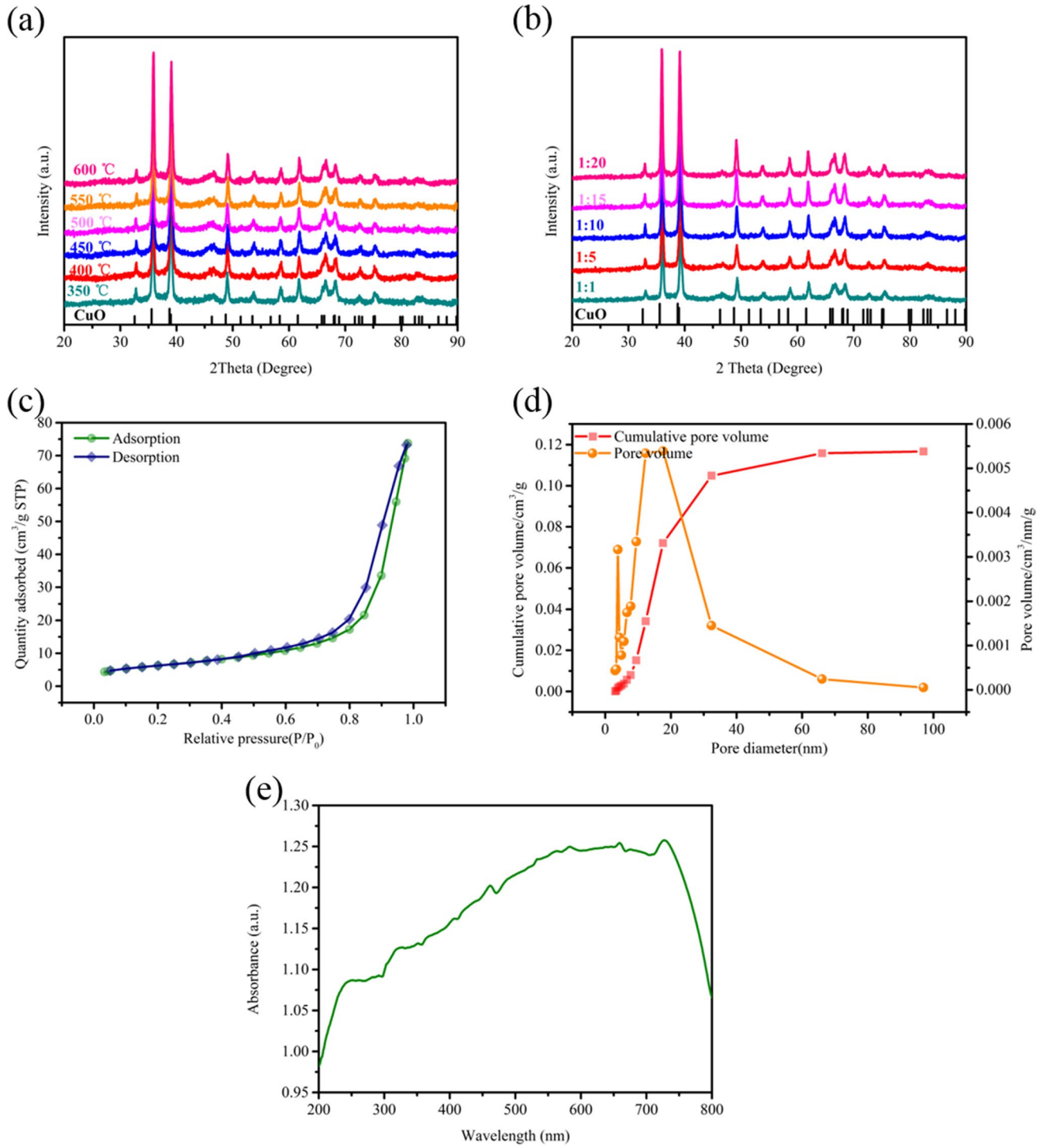

Fig. 2 XRD patterns of CuO@γ-Al2O3(1:15)-350, CuO@γ-Al2O3(1:15)-400, CuO@γ-Al2O3(1:15)-450, CuO@γ-Al2O3(1:15)-500, CuO@γ-Al2O3(1:15)-550, and CuO@γ-Al2O3(1:15)-600 (**a**); XRD patterns of CuO@γ-Al2O3(1:1)-450, CuO@γ-Al2O3(1:5)-450, CuO@γ-Al2O3(1:10)-450, CuO@γ-Al2O3(1:15)-450, and CuO@γ-Al2O3(1:20)-450 (**b**); nitrogen adsorption–desorption isotherms (**c**); pore size distribution (**d**); and UV − vis DRS spectrum (**e**) of the CuO@γ-Al2O3(1:15)-450 nanocomposite catalyst

the (110), (-111), (111), (-202), (-113), (113), and (220) characteristic peaks observed at approximately 32.534°, 35.558°, 38.753°, 48.752°, 61.569°, 67.971°, and 68.142°, respectively, indicate the formation of CuO (Wang et al. 2021). From the XRD analysis, we concluded that CuO was generated irrespective of the calcination temperature (350 °C, 400 °C, 450 °C, 500 °C, 550 °C, or 600 °C) and the mass ratio of γ-Al_2O_3:$Cu(NO_3)_2{\cdot}3H_2O$ (1:1, 1:5, 1:10, 1:15, or 1:20).

The N_2 adsorption–desorption isotherms and pore size distribution of the CuO@γ-Al_2O_3(1:15)-450 nanocomposite catalyst are shown in Fig. 2(c) and Fig. 2(d), respectively. The obtained isotherms, which exhibited type IV characteristics, and pore size distribution implied the existence of mesoporous structures in the synthesized nanocomposites (Ding et al. 2018; Raees et al. 2021). The mesoporous CuO@γ-Al_2O_3(1:15)-450 nanocomposite exhibited a large specific surface area and high pore volume, which were mainly due to the mesoporous structure; these values were 22.444 m^2/g and 0.117 cm^3/g, respectively. The large specific surface area and high pore volume of the mesoporous CuO@γ-Al_2O_3 nanocomposite were expected to increase the removal rate of PVA.

The UV–vis diffuse reflectance spectrum of the CuO@γ-Al_2O_3(1:15)-450 nanocomposite catalyst was obtained to investigate its optical properties. As shown in Fig. 2(e), the catalyst exhibits excellent absorption in the visible wavelength range (500–700 nm).

XPS characterization

The chemical composition and surface chemical state of the prepared CuO@γ-Al_2O_3(1:15)-450 nanocomposite catalyst (fresh and used) were studied by X-ray photoelectron spectroscopy (XPS). Figure 3 clearly shows that the Fenton-like reaction has no effect on the chemical elements in the CuO@γ-Al_2O_3(1:15)-450 catalyst. This shows that the CuO@γ-Al_2O_3(1:15)-450 catalyst has high chemical stability. The results of XPS analysis indicated that the sample contained O, Cu, and Al elements (Fig. 3(a)). The high-resolution Cu 2p XPS spectrum (Fig. 3(d)) further indicates that the peaks at 933.34 eV and 953.19 eV correspond to 2p3/2 and 2p1/2 of the Cu atoms in the CuO structure. Simultaneously, the peaks located at approximately 941.35 eV, 943.96 eV, 961.38 eV, and 962.38 eV corresponded to the strong Cu^{2+} satellite peaks. Figure 3(c) shows the spectra of pure CuO (black line) and the CuO@γ-Al_2O_3 nanocomposite catalyst (fresh: purple line; used: green line), and we can observe that the spectra basically coincide; this indicated that the CuO@γ-Al_2O_3 nanocomposites were formed after calcination. The O 1 s spectra are shown in Fig. 3(b). The peak at 531.1 eV was relatively strong, which might be due to the adsorption of hydroxyl groups; the peak at 529.74 eV may represent the lattice oxygen (O^{2-}), and the peak at 533.2 eV may correspond to H_2O (Shuang et al. 2020). Therefore, the XPS analysis further confirmed that this irregular structure was the CuO@γ-Al_2O_3 nanocomposite.

Photocatalytic performance and reusability

The photocatalytic degradation of PVA was used to assess the photocatalytic performance of the synthesized CuO@γ-Al_2O_3 nanocomposite catalysts. In this study, we discussed the effect of calcination temperature, mass ratio of γ-Al_2O_3:$Cu(NO_3)_2{\cdot}3H_2O$, pH value, catalyst dosage, H_2O_2 dosage, and different systems on PVA degradation. The reaction time was 120 min, and the reaction temperature was 20 °C for all degradation reactions. The results are discussed below.

Effect of calcination temperature

Figure 4(a–b), Table S2, Fig. S2(a), and Fig. S3(a) indicate the effect of the calcination temperature on the PVA removal rate and TOC removal rate. The other reaction conditions are as follows: mass ratio of γ-Al_2O_3:$Cu(NO_3)_2{\cdot}3H_2O$, 1:15; pH value, 7; catalyst dosage, 2.6 g/L; and H_2O_2 dosage, 0.2 g/mL. When the calcination temperature increased from 350 to 450 °C, the PVA removal rate, TOC removal rate, and k value increased from 92.7 to 99.21%, 87.69 to 94.57%, and 0.02357 to 0.04183 min^{-1}, respectively. When the calcination temperature increased from 450 to 600 °C, the PVA removal rate, TOC removal rate, and k value were almost unchanged. This indicated that when the calcination temperature was higher than 450 °C, the catalytic activity of CuO was the highest, and a stable mesoporous structure could be formed on the catalyst surface (Ahn et al. 2016). When the calcination temperature was lower than 450 °C, the active components may not be able to form strong structures, resulting in reduced catalytic efficiency (Su et al. 2019; Dong et al. 2020). To test this inference, we performed metal leaching experiments. The experimental results are shown in Table S3. When the calcination temperature was higher than 450 °C, the concentration of leached Cu ions significantly decreased to 0.12 mg/L. This value was less than the concentrations observed at 350 °C (0.183 mg/L) and 400 °C (0.145 mg/L).

Effect of the mass ratio of γ-Al_2O_3:$Cu(NO_3)_2{\cdot}3H_2O$

The mass ratio of γ-Al_2O_3:$Cu(NO_3)_2{\cdot}3H_2O$ always has a significant effect on photocatalytic activity, especially for catalysts. Therefore, to determine the effect of the mass ratio of γ-Al_2O_3:$Cu(NO_3)_2{\cdot}3H_2O$, five mass ratios, i.e., 1:1, 1:5, 1:10, 1:15, and 1:20, were investigated under visible light irradiation. The other reaction conditions are as follows: calcination temperature, 450 °C; pH value,

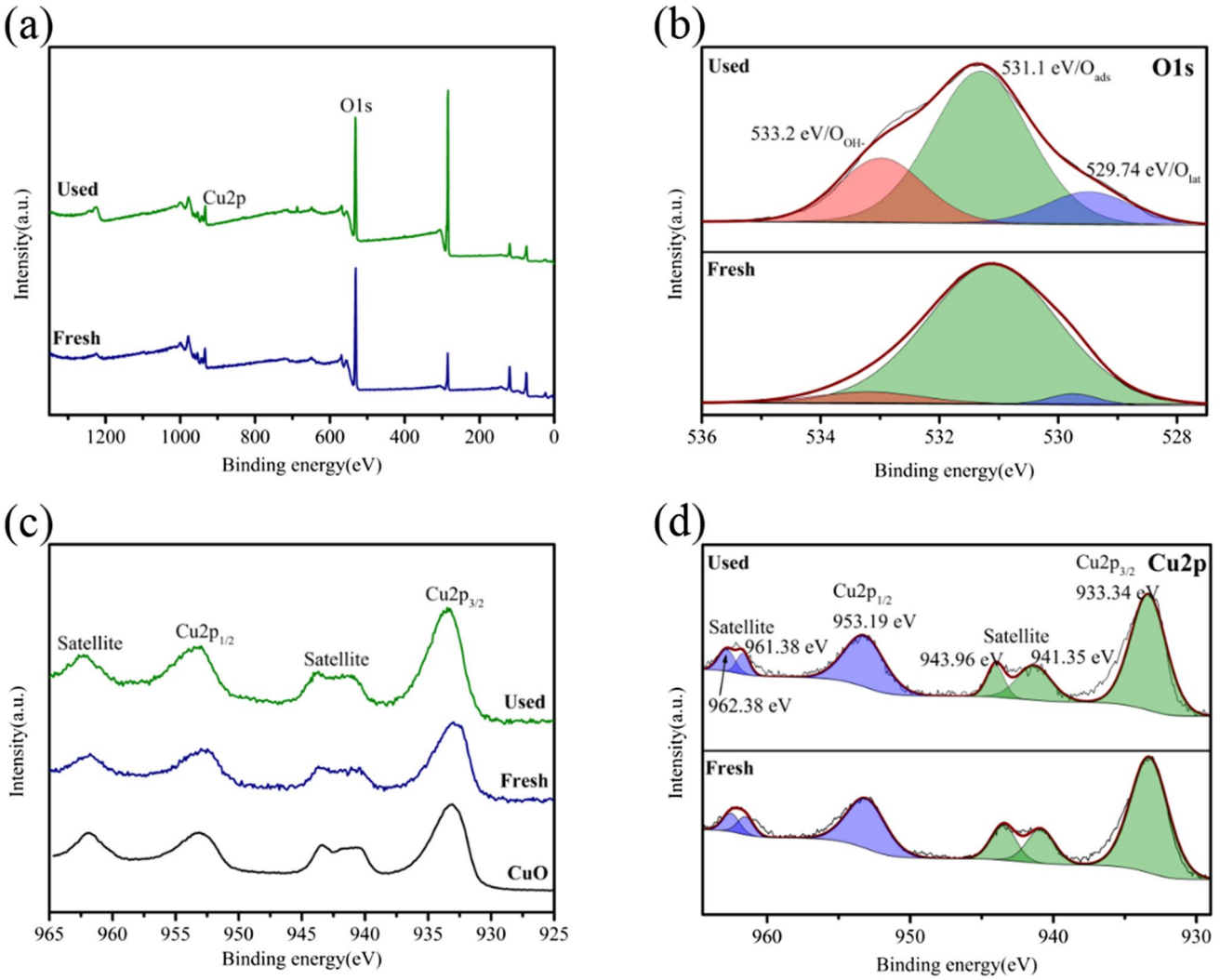

Fig. 3 XPS spectra (before use and after use) of the CuO@γ-Al2O3(1:15)-450 nanocomposite catalyst (**a**); O 1 s (**b**), CuO (**c**), and Cu 2p (**d**) spectra

7; catalyst dosage, 2.6 g/L; and H_2O_2 dosage, 0.2 g/mL. As illustrated in Fig. 4(c–d), Table S4, Fig. S2(b), and Fig. S3(b), after 120 min, the PVA removal rate, TOC removal rate, and *k* value increased to 99.21%, 94.57%, and 0.04183 min^{-1}, respectively. When the mass ratio of γ-Al_2O_3:$Cu(NO_3)_2{\cdot}3H_2O$ was further increased, the PVA removal rate and TOC removal rate did not increase further. Theoretically, the more the $Cu(NO_3)_2{\cdot}3H_2O$ added, the more the active sites produced (Liang et al. 2021; Li et al. 2021b). However, the excessive addition of $Cu(NO_3)_2{\cdot}3H_2O$ did not further increase the PVA removal rate. This was because the active sites of the γ-Al_2O_3 carrier were saturated. When the active sites of a carrier are saturated, the catalytic activity does not increase further. Accordingly, based on the catalytic efficiency, the best mass ratio of γ-Al_2O_3:$Cu(NO_3)_2{\cdot}3H_2O$ was considered as 1:15 in the subsequent catalytic experiments.

Effect of pH value

An appropriate pH value of the reaction solution is of great significance for the practical applications of photocatalysis experiments; thus, the pH values of 3, 4, 5, 6, 7, 8, 9, and 10 were explored to investigate the effect of pH on the catalytic reaction. The other reaction conditions are as follows: calcination temperature, 450 °C; mass ratio of γ-Al_2O_3:$Cu(NO_3)_2{\cdot}3H_2O$, 1:15; catalyst dosage, 2.6 g/L; and H_2O_2 dosage, 0.2 g/mL. Figure 5(a–b), Table S5, Fig. S2(c), and Fig. S3(c) indicate that when the pH value increased from 3 to 7, the PVA removal rate, TOC removal rate, and *k* value increased from 98.224, 94.71, and 0.03382 to 99.21%, 94.57%, and 0.04183 min^{-1}, respectively. When the pH value increased from 7 to 10, the PVA removal rate, TOC removal rate, and *k* value decreased to

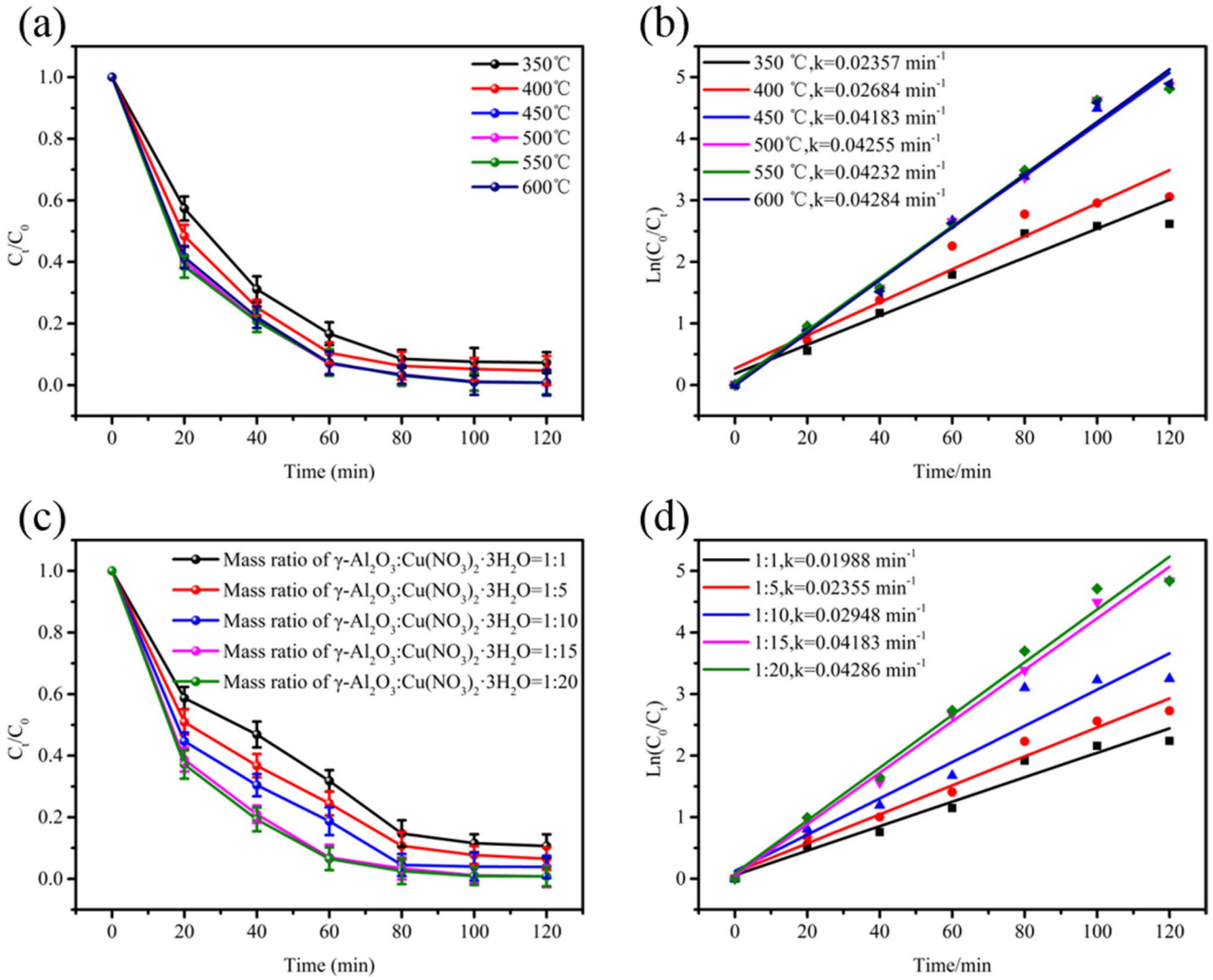

Fig. 4 Effects of calcination temperature (**a**–**b**) and mass ratio of γ-Al2O3:Cu(NO3)2·3H2O (**c**–**d**) on PVA degradation

32.374%, 28.79%, and 0.00325 min^{-1}, respectively. Thus, the increase in the pH value from 7 to 10 considerably reduced the PVA removal rate, TOC removal rate, and *k* value, indicating that the CuO@γ-Al_2O_3 nanocomposite catalyst has very low catalytic activity under alkaline conditions. Under light irradiation, the CuO@γ-Al_2O_3 nanocomposite catalyst produced oxidative species, such as ·OH radicals. These free radicals and H_2O_2 easily decompose under alkaline conditions but exhibit better stability under acidic or neutral conditions (Li et al. 2019b; Kanjana et al. 2020). Therefore, the catalyst could provide the best oxidation performance under acidic or neutral conditions and improve the photocatalytic removal rate (Shang et al. 2012; Wang et al. 2020a). The pH experiments showed that the CuO@γ-Al_2O_3 nanocomposite catalyst has excellent catalytic activity under acidic or neutral conditions.

Effect of catalyst dosage

To investigate the effect of catalyst dosage on photocatalytic activity, five catalyst dosages, i.e., 1.4 g/L, 1.8 g/L, 2.2 g/L, 2.6 g/L, and 3 g/L, were used for PVA degradation under visible light irradiation for 120 min. The results are shown in Fig. 5(c–d), Table S6, Fig. S2(d), and Fig. S3(d). The other reaction conditions are as follows: calcination temperature, 450 °C; mass ratio of γ-Al_2O_3:$Cu(NO_3)_2$·3H_2O, 1:15; pH value, 7; and H_2O_2 dosage, 0.2 g/mL. When the catalyst dosage was increased from 1.4 to 2.6 g/L, the PVA removal rate, TOC removal rate, and *k* value increased from 87.64, 83.36, and 0.01777 to 99.21%, 94.57%, and 0.04183 min^{-1}, respectively. When the catalyst dosage was further increased, the PVA removal rate and TOC removal rate did not increase further. This indicated that with the

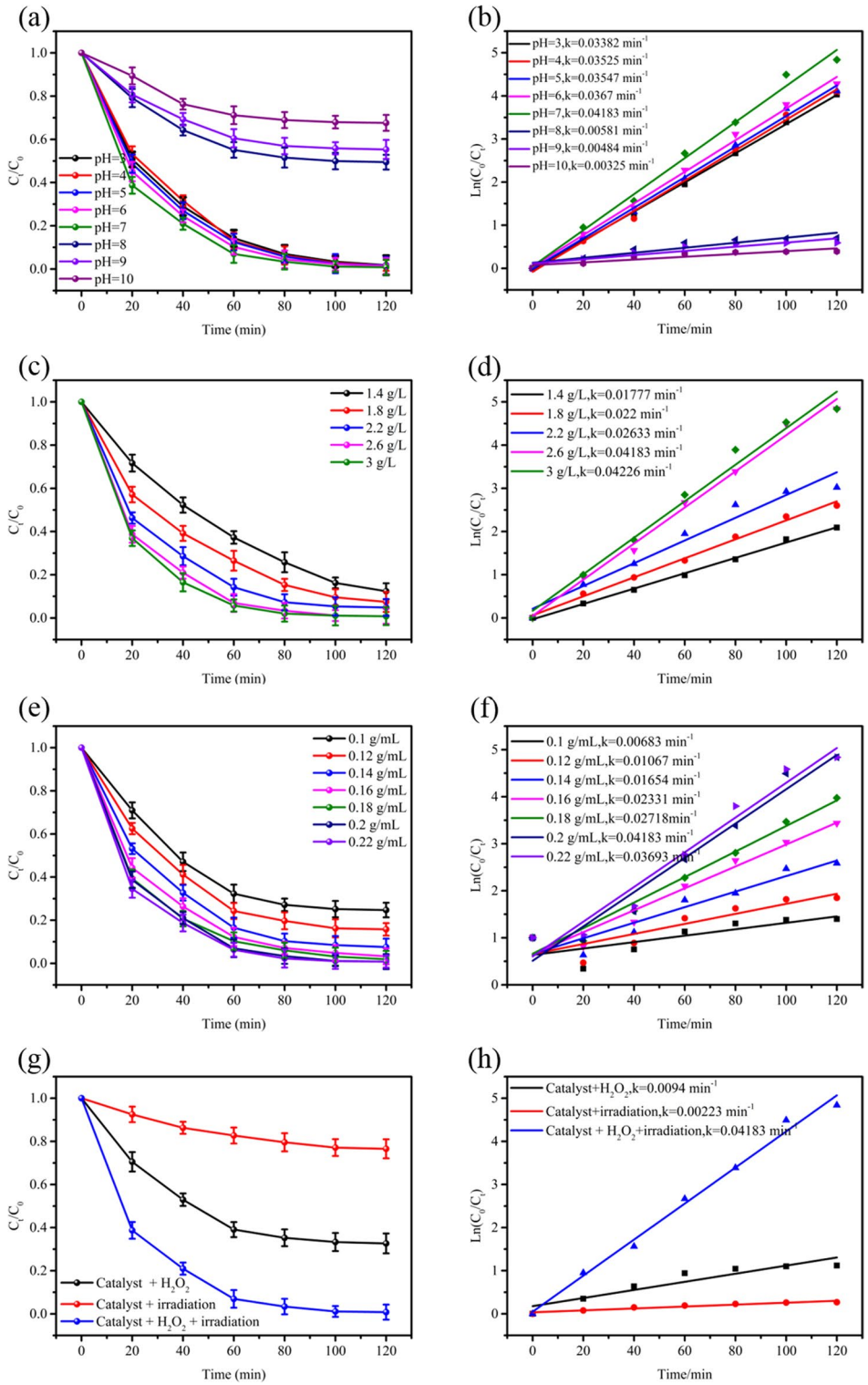

Fig. 5 Effects of initial pH (**a**–**b**), catalyst dosage (**c**–**d**), H2O2 dosage (**e**–**f**), and different systems (**g**–**h**) on PVA degradation

increase in the catalyst dosage, the active sites of the catalytic reaction increased, and the ·OH radicals generated per unit time also increased correspondingly (Raees et al. 2021; Islam et al. 2021). When the catalyst dosage was more than 2.6 g/L, the PVA removal rate and TOC removal rate did not increase further because of the low H_2O_2 concentration in the reaction solution, due to which more ·OH radicals could not be generated (Kadi et al. 2020; Li et al. 2021a). In summary, these results confirmed that the best catalyst dosage was 2.6 g/L.

Effect of H_2O_2 dosage

The concentration of the H_2O_2 oxidant plays a vital role in the catalytic process because it is directly related to the number of generated ·OH radicals. The effects of H_2O_2 dosage (0.1 g/mL, 0.12 g/mL, 0.14 g/mL, 0.16 g/mL, 0.18 g/mL, 0.2 g/mL, and 0.22 g/mL) on the PVA removal rate and TOC removal rate were investigated in this study. The other reaction conditions are as follows: calcination temperature, 450 °C; mass ratio of γ-Al_2O_3:$Cu(NO_3)_2$·3H_2O, 1:15; pH value, 7; and catalyst dosage, 2.6 g/L. The results are shown in Fig. 5(e–f), Table S6, Fig. S2(e), and Fig. S3(e). When the H_2O_2 dosage was increased from 0.1 to 0.2 g/mL, the PVA removal rate, TOC removal rate, and *k* value increased from 75.31, 70.89, and 0.00683 to 99.21%, 94.57%, and 0.04183 min^{-1}, respectively. When the H_2O_2 dosage was further increased, the PVA removal rate and TOC removal rate did not increase further. In general, the amount of ·OH radicals produced is proportional to the concentration of H_2O_2; that is, the higher the concentration of H_2O_2, the higher the amount of the ·OH radicals produced; consequently, the removal rate of the pollutant increases (Gholizadeh et al. 2020; Bagtache et al. 2021). However, when the concentration of H_2O_2 exceeds the critical value, the excess H_2O_2 reacts with hydroxyl radicals and converts the hydroxyl radicals into hydroperoxyl radicals; consequently, the removal rate may decrease (Esmaeili et al. 2020; Chen et al. 2020c, p.; Muthukrishnaraj et al. 2020). The optimal concentration of H_2O_2 was 0.2 g/mL because of its fast removal rate and no excessive consumption of oxidants.

Effect of different systems

In this study, we also investigated the effects of three different systems (catalyst + H_2O_2, catalyst + irradiation, and catalyst + H_2O_2 + irradiation) on the removal rate of PVA; the experimental results are exhibited in Fig. 5(g–f), Fig. S2(f), and Fig. S3(f). For the catalyst + H_2O_2 system, the PVA removal rate, TOC removal rate, and *k* value were 67.35%, 62.47%, and 0.0094 min^{-1}, respectively, after 120 min. This indicated that the CuO@γ-Al_2O_3 nanocomposite catalyst exhibited unsatisfactory performance for the degradation of PVA under dark conditions. Under the catalysis of CuO, only a small amount of H_2O_2 decomposed to produce ·OH radicals (Ding et al. 2018; Su et al. 2019; Akram et al. 2021), as shown in Eqs. (4) and (5):

$$Cu^{2+} + H_2O_2 \rightarrow Cu^{+} + O_{2^-} + 2H^{+} \quad (4)$$

$$Cu^{+} + H_2O_2 \rightarrow Cu^{2+} + \cdot OH + OH^{-} \quad (5)$$

Without the addition of H_2O_2, it was observed that the PVA removal rate, TOC removal rate, and *k* value were 23.46%, 18.56%, and 0.00223 min^{-1}, respectively, after 120 min. This shows that without adding H_2O_2, the catalyst can generate free radicals through irradiation to achieve the degradation of PVA. For the catalyst + H_2O_2 + irradiation system, the PVA removal rate, TOC removal rate, and *k* value were 99.21%, 94.57%, and 0.04183 min^{-1}, respectively. The experimental results indicated that under the conditions of both visible light irradiation and H_2O_2, the reaction system exhibited excellent performance for the degradation of PVA.

Reusability

The stability and reusability of materials are important aspects to evaluate their practical applications. To investigate the reusability of the CuO@γ-Al_2O_3 nanocomposite catalyst, ten photodegradation experiments were conducted (calcination temperature, 450 °C; mass ratio of γ-Al_2O_3:$Cu(NO_3)_2$·3H_2O, 1:15; pH value, 7; catalyst dosage, 2.6 g/L; reaction temperature, 20 °C; and H_2O_2 dosage, 0.2 g/mL). The results are shown in Fig. 6. For the ten cycles, the PVA removal rates were 99.21%, 99.07%, 98.94%, 98.83%, 98.616%, 98.543%, 98.327%, 98.105%, 97.897%, and 97.582%, respectively (Fig. 6(a)); furthermore, the TOC removal rates were 94.57%, 94.31%, 93.97%, 93.68%, 93.41%, 93.19%, 92.99%, 92.71%, 92.49%, and 92.18%, respectively (Fig. 6(b)). Even though there was a slight decrease in the PVA removal rate and TOC removal rate during the ten cycles, the values were still higher than 97% and 92%, respectively. The slight decrease in the PVA removal rate was probably due to the following two reasons: (1) The degradation intermediates blocked the mesopores of the catalyst; (2) during the photodegradation process, the quantity of the CuO@γ-Al_2O_3 nanocomposite catalyst decreased after centrifugation, separation, and drying, thereby reducing the number of active sites. However, the satisfactory PVA removal rate and TOC removal rate after ten cycles indicated the excellent reusability of the CuO@γ-Al_2O_3 nanocomposite catalyst. The concentrations of leached Cu ions in the solutions were measured after each degradation experiment. Figure 6(c) shows that about 0.12 mg/L of Cu ions leached in 120 min in the first cycle, accounting for 0.005% of the total amount in the CuO@γ-Al_2O_3 nanocomposite catalyst. Furthermore, about 0.032 mg/L Cu ions leached in the tenth cycle. The XRD results (Fig. 6(d)) indicated that the reused CuO@γ-Al_2O_3 nanocomposite catalyst could maintain its crystalline phase after 10 catalytic cycles.

Practical applications of the CuO@γ-Al_2O_3 nanocomposite catalyst

According to the abovementioned characteristics and performance analysis, it can be inferred that the CuO@γ-Al_2O_3 nanocomposite catalyst has high photocatalytic activity. In order to further verify this inference, the highly toxic printing and dyeing wastewater containing rhodamine B and reactive red X-3B was obtained for the degradation experiments, and the CuO@γ-Al_2O_3 nanocomposite catalyst was used for the photocatalytic degradation of rhodamine B and reactive red X-3B. The reaction conditions are as follows: calcination temperature, 450 °C; mass ratio of γ-Al_2O_3:$Cu(NO_3)_2$·$3H_2O$, 1:15; pH value, 7; catalyst dosage, 2.6 g/L; reaction temperature, 20 °C; and H_2O_2 dosage, 0.2 g/mL. After photocatalytic degradation for 120 min, the removal rates of rhodamine B and reactive red X-3B were 99.91% and 99.25%, respectively (Fig. 7(e)). Figure 7(a–b) and Fig. 7(c–d) show the temporal changes in the UV–vis spectra of the aqueous solutions of rhodamine B and reactive red X-3B in the range of 200–700 nm. The absorption peaks detected at 554 nm and 539 nm correspond to rhodamine B and reactive red X-3B; it can be seen that the intensities of both absorption peaks decreased with the reaction time, and the peaks almost disappeared after 120 min. Therefore, it can be concluded that the CuO@γ-Al_2O_3 nanocomposite catalyst has high photocatalytic activity for the treatment of printing and dyeing wastewater. Furthermore, rhodamine B and reactive red X-3B can be effectively degraded and decolorized and finally completely mineralized into small molecules such as CO_2 and H_2O through photocatalytic redox reactions (Chen et al. 2020d).

Possible catalytic mechanism

On the basis of the experimental results, a mechanism for the photocatalytic degradation of PVA, rhodamine B, and reactive red X-3B by the CuO@γ-Al_2O_3 nanocomposite

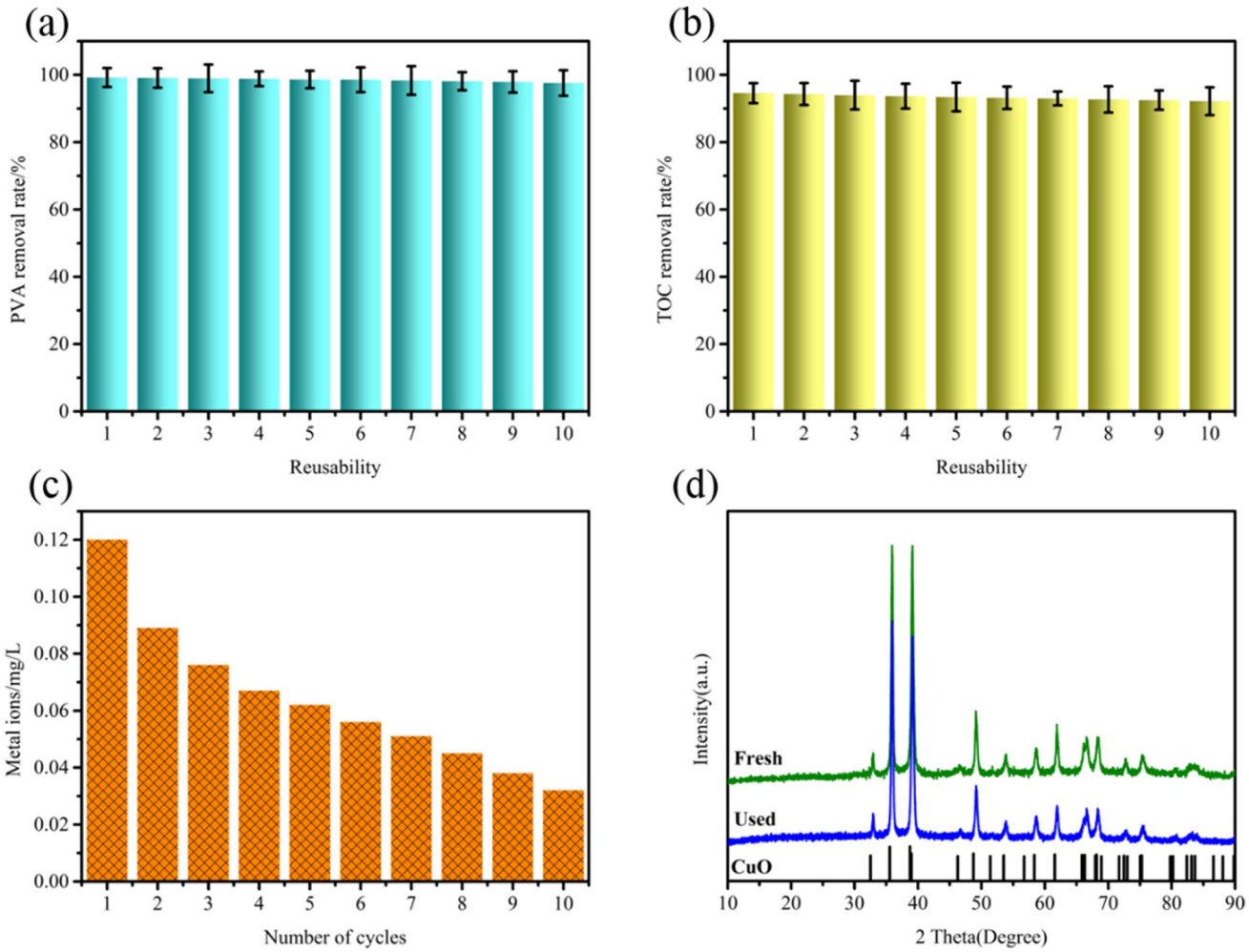

Fig. 6 Reusability of CuO@γ-Al2O3 (**a**–**b**); leaching of Cu ions during the PVA degradation process (**c**); and XRD patterns (**d**: fresh and used)

catalyst was proposed (Fig. 8). In the photocatalytic reaction, the photogenerated electrons transfer from the valence band (VB) to the conduction band (CB) (Dong et al. 2020; Raees et al. 2021). The transferred electrons react with H_2O_2 and O_2 to generate ·OH and $\cdot O_2^-$ radicals (Li et al. 2020b; Chen et al. 2020c; Abdelaal et al. 2020; Muthukrishnaraj et al. 2020), which participate in the removal of PVA, rhodamine B, and reactive red X-3B. At the same time, the holes accumulated in the VB of the CuO@γ-Al_2O_3 nanocomposite catalyst have sufficient energy to oxidize H_2O to generate ·OH radicals (Abdelaal et al. 2020; Muthukrishnaraj et al. 2020; Bielan et al. 2021). The photocatalytic process may include the following elementary steps (Kamat 2017; Colmenares et al. 2017; Strieth-Kalthoff et al. 2018; Xiao et al. 2019; Zhang et al. 2020):

$$\mathrm{CuO@\gamma{-}Al_2O_3\ nanocomposite\ catalyst + hv \rightarrow CuO@\gamma - Al_2O_3\ nanocomposite\ catalyst\ (h^+ + e^-)} \quad (6)$$

$$H_2O + h^+ \rightarrow HO^- + H^+ \quad (7)$$

$$HO^- + h^+ \rightarrow \cdot OH \quad (8)$$

$$O_2 + e^- \rightarrow \cdot O_2^- \quad (9)$$

$$O_2^- + H^+ \rightarrow HO_2 \quad (10)$$

$$HO_2 \cdot + HO_2 \cdot \rightarrow H_2O_2 + O_2 \quad (11)$$

$$HO_2 \cdot + \cdot O_2^- \rightarrow HO_2^- + O_2 \quad (12)$$

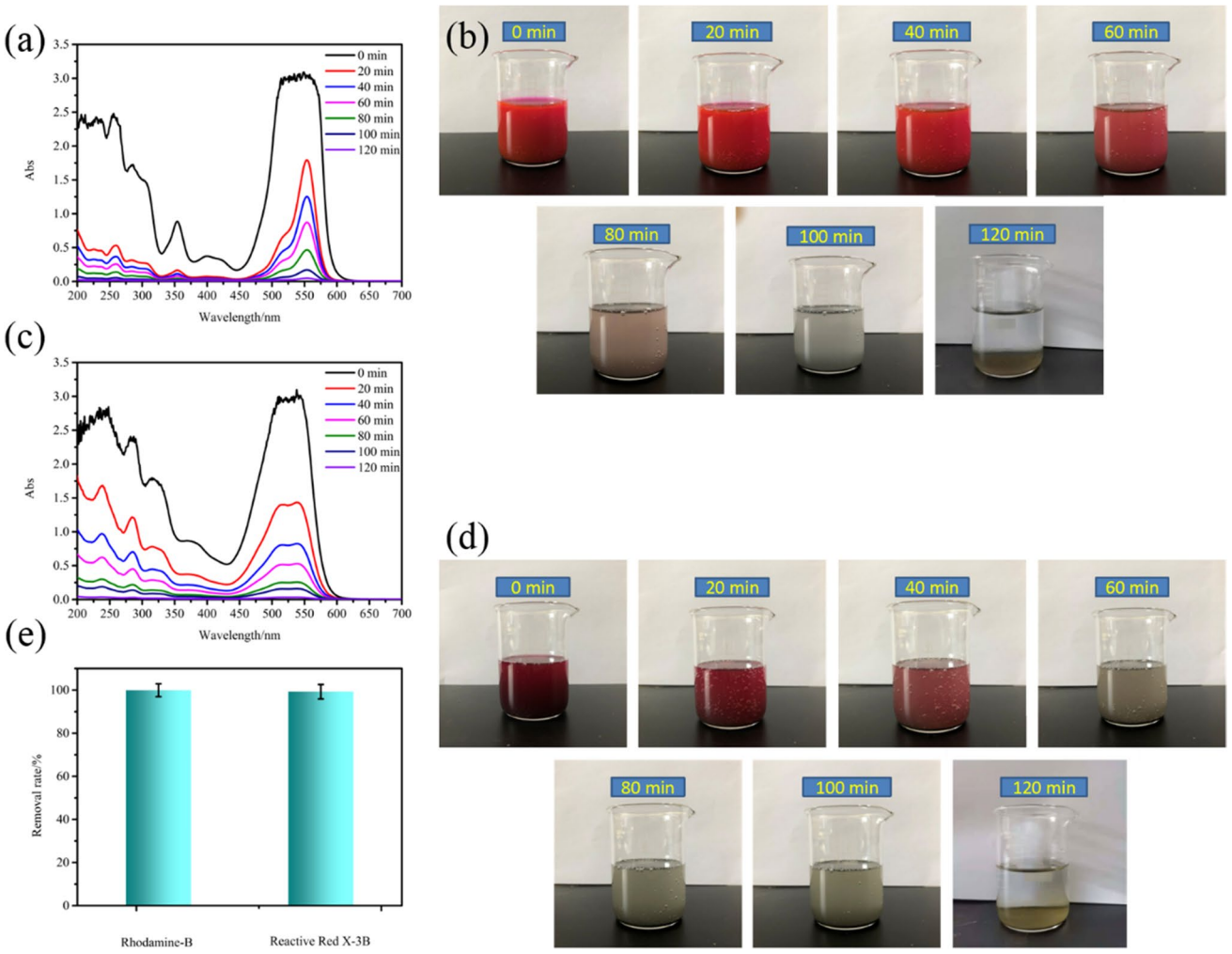

Fig. 7 Time-dependent UV–vis absorption spectra and images of rhodamine B (**a**–**b**, respectively) and reactive red X-3B (**c**–**d**, respectively); removal rates of rhodamine B and reactive red X-3B (**e**)

$$HO_2^- \cdot + H^+ \rightarrow H_2O_2 \quad (13)$$

$$H_2O_2 + \cdot O_2^- \rightarrow \cdot OH + HO^- + O_2 \quad (14)$$

$$H_2O_2 + e^- \rightarrow \cdot OH + HO^- \quad (15)$$

$$H_2O_2 + hv \rightarrow 2 \cdot OH \quad (16)$$

$$HO_2 \cdot \rightarrow H^+ + O2^- \quad (17)$$

$$2O_2^- + 2H_2O \rightarrow {}^1O_2 + H_2O_2 + 2OH^- \quad (18)$$

$$h/e-/\cdot OH/O_2^-/{}^1O_2 + \text{PVA/rhodamine B /Reactive Red X} - 3B \rightarrow H_2O + CO_2 \quad (19)$$

Another important aspect of the prepared CuO@γ-Al_2O_3 nanocomposite catalyst is the ability to generate ·OH radicals, which can be generated in Fenton-like and photocatalytic reactions; these ·OH radicals can synergistically degrade PVA, rhodamine B, and reactive red X-3B. In the Fenton-like reaction, Cu^{2+} reacts with H_2O_2 to produce $\cdot O_2^-$. Then, H_2O_2 oxidizes Cu^+ to Cu^{2+}, generating ·OH. In this process, Cu^+ and Cu^{2+} rapidly react with H_2O_2, which promotes the Cu^+/Cu^{2+} cycle (Akram et al. 2021; Wang et al. 2021). In addition, the presence of electrons is conducive to the generation of ·OH and $\cdot O_2^-$ radicals in the Fenton-like process (Yang and Wang 2018; Abudayyeh et al. 2021); they considerably increase the number of active groups and further enhance the photoactivity. The detailed mechanism of the Fenton-like reaction can be summarized as Eqs. (4) and (5).

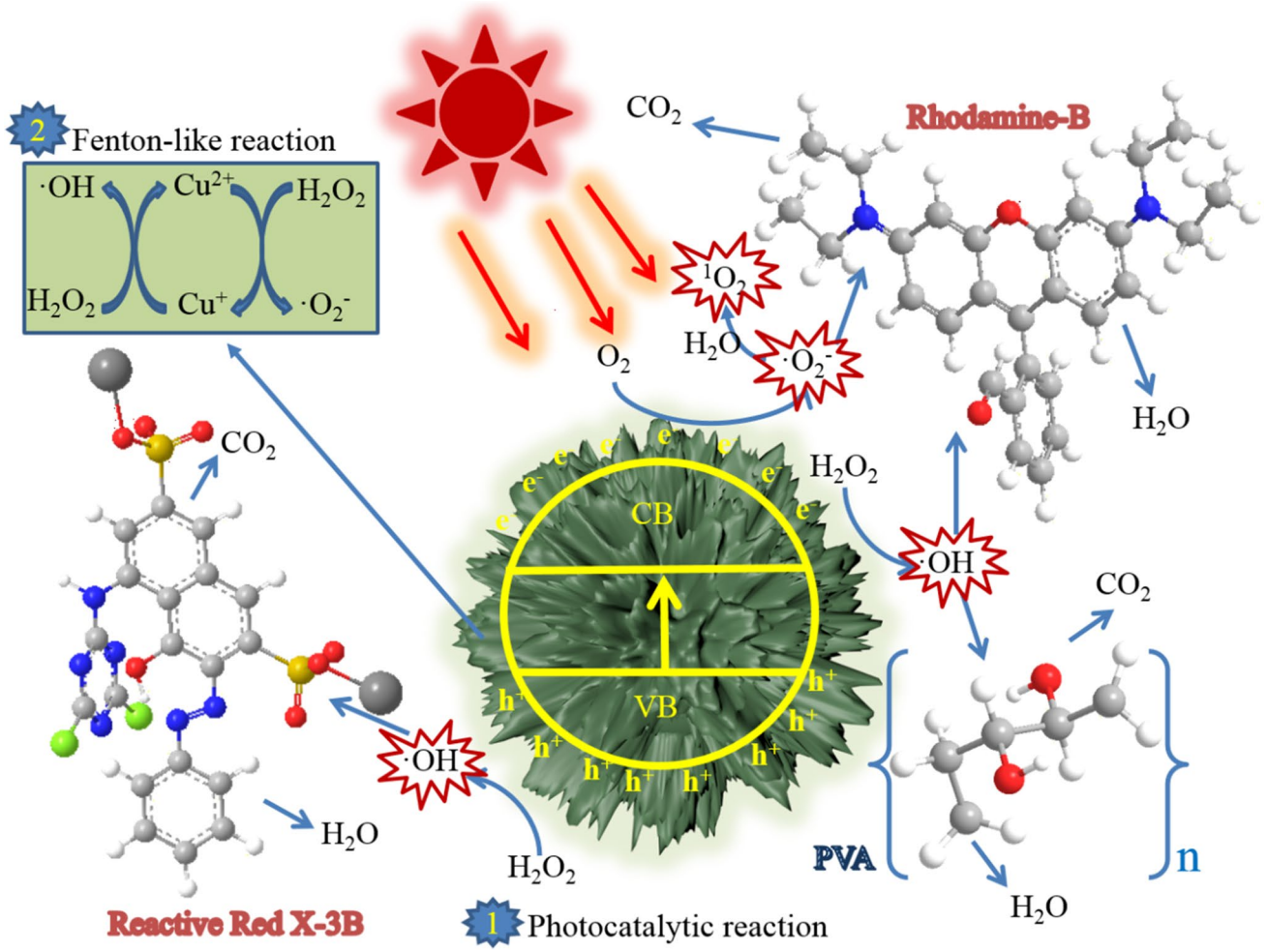

Fig. 8 A schematic of the feasible mechanism of the photocatalytic reaction

Conclusion

In summary, a photocatalytic Fenton-like system was constructed, in which visible light and H_2O_2 were used as the external driving energy and raw material, respectively. This system exhibited excellent performance for the degradation of PVA. At the same time, the system also exhibited wide applications as well as stability for the degradation of rhodamine B and reactive red X-3B. The efficient utilization of H_2O_2 led to the continuous generation of abundant ·OH radicals, which resulted in high efficiency and high degradation and mineralization ability of the photocatalyst. This remarkable catalytic performance may be due to the synergistic effect of the photocatalytic reaction and the Fenton-like reaction. This study provides an efficient and easy-to-operate method for treating wastewater containing PVA and dyes.

Supplementary Information The online version contains supplementary material available at https://doi.org/10.1007/s11356-022-20698-w.

Author contributions Gaofeng Zhu: conceptualization, methodology, software, formal analysis, writing – original draft. Yang Jin: funding acquisition, formal analysis. Mingqiao Ge: writing – review and editing, supervision, funding acquisition.

Funding We gratefully acknowledge the support of this research by the Natural Science Foundation of Jiangsu Province (BK20200620), Natural Science Foundation of China (52103140), National High-tech R&D Program of China (No.2016YFB0302901), nand Fundamental Research Funds for the Central Universities (No.JUSRP51723B) for the financial support of the work.

Data availability The datasets used during the current study are available from the corresponding author on reasonable request.

Declarations

Ethics approval and consent to participate Not applicable.

Consent for publication Not applicable.

Competing interests The authors declare no competing interests.

References

Abdelaal HM, Shaikjee A, Esmat M (2020) High performing photocatalytic ZnO hollow sub-micro-spheres fabricated by microwave induced self-assembly approach. Ceram Int 46:19815–19821. https://doi.org/10.1016/j.ceramint.2020.05.034

Abudayyeh AM, Schott O, Feltham HLC et al (2021) Copper catalysts for photo- and electro-catalytic hydrogen production. Inorg Chem Front 8:1015–1029. https://doi.org/10.1039/d0qi01247e

Aghayi-Anaraki M, Safarifard V (2020) Fe3O4@MOF Magnetic nanocomposites: synthesis and applications. Eur J Inorg Chem 2020:1916–1937. https://doi.org/10.1002/ejic.202000012

Agu UA, Mendieta SN, Gerbaldo M et al (2020) Highly active heterogeneous Fenton-like system based on cobalt ferrite. Ind Eng Chem Res 59:1702–1711. https://doi.org/10.1021/acs.iecr.9b04042

Ahn K, Pham-Cong D, Choi HS et al (2016) Bandgap-designed TiO2/SnO2 hollow hierarchical nanofibers: Synthesis, properties, and their photocatalytic mechanism. Curr Appl Phys 16:251–260. https://doi.org/10.1016/j.cap.2015.12.006

Akram N, Ma W, Guo J et al (2021) Synergistic catalysis of Fe3O4/CuO bimetallic catalyst derived from Prussian blue analogues for the efficient decomposition of various organic pollutants. Chem Phys 540:110974. https://doi.org/10.1016/j.chemphys.2020.110974

Ali I, Alharbi OML, Alothman ZA, Badjah AY (2018) Kinetics, thermodynamics, and modeling of amido black dye photodegradation in water using Co/TiO_2 nanoparticles. Photochem Photobiol 94:935–941. https://doi.org/10.1111/php.12937

Ali I, Burakov AE, Melezhik AV et al (2019) Removal of copper(II) and zinc(II) ions in water on a newly synthesized polyhydroquinone/graphene nanocomposite material: kinetics, thermodynamics and mechanism. ChemistrySelect 4:12708–12718. https://doi.org/10.1002/slct.201902657

Ali I, Afshinb S, Poureshgh Y et al (2020) Green preparation of activated carbon from pomegranate peel coated with zero-valent iron nanoparticles (nZVI) and isotherm and kinetic studies of amoxicillin removal in water. Environ Sci Pollut Res 27:36732–36743. https://doi.org/10.1007/s11356-020-09310-1

Ali I, Babkin AV, Burakova IV et al (2021) Fast removal of samarium ions in water on highly efficient nanocomposite based graphene oxide modified with polyhydroquinone: Isotherms, kinetics, thermodynamics and desorption. J Mol Liq 329:115584. https://doi.org/10.1016/j.molliq.2021.115584

Ali I, Konkova T, Kasianov V et al (2021) Preparation and characterization of nano-structured modified montmorillonite for dioxidine antibacterial drug removal in water. J Mol Liq 331:115770. https://doi.org/10.1016/j.molliq.2021.115770

Bagtache R, Meziani D, Abdmeziem K, Trari M (2021) Synthesis, physical and photo-electrochemical characterizations of a new hybrid host-guest complex [Cu-12(C2N3H2)(8)Cl][(PW12O40)]. J Mol Struct 1227:129718. https://doi.org/10.1016/j.molstruc.2020.129718

Basheer AA (2018) New generation nano-adsorbents for the removal of emerging contaminants in water. J Mol Liq 261:583–593. https://doi.org/10.1016/j.molliq.2018.04.021

Basheer AA (2020) Advances in the smart materials applications in the aerospace industries. AEAT 92:1027–1035. https://doi.org/10.1108/AEAT-02-2020-0040

Behnajady MA, Modirshahla N, Ghanbary F (2007) A kinetic model for the decolorization of CI Acid Yellow 23 by Fenton process. J Hazard Mater 148:98–102. https://doi.org/10.1016/j.jhazmat.2007.02.003

Bian H, Cao M, Wen H et al (2019) Biodegradation of polyvinyl alcohol using cross-linked enzyme aggregates of degrading enzymes from Bacillus niacini. Int J Biol Macromol 124:10–16. https://doi.org/10.1016/j.ijbiomac.2018.11.204

Bielan Z, Kowalska E, Dudziak S et al (2021) Mono- and bimetallic (Pt/Cu) titanium(IV) oxide core-shell photocatalysts with UV/Vis light activity and magnetic separability. Catal Today 361:198–209. https://doi.org/10.1016/j.cattod.2020.05.034

Chen R, Fan F, Dittrich T, Li C (2018) Imaging photogenerated charge carriers on surfaces and interfaces of photocatalysts with surface photovoltage microscopy. Chem Soc Rev 47:8238–8262. https://doi.org/10.1039/c8cs00320c

Chen BB, Liu ML, Huang CZ (2020) Carbon dot-based composites for catalytic applications. Green Chem 22:4034–4054. https://doi.org/10.1039/d0gc01014f

Chen D, Liu C, Lu J et al (2020) Enhanced phycocyanin and DON removal by the synergism of H2O2 and micro-sized ZVI: optimization, performance, and mechanisms. Sci Total Environ 738:140134. https://doi.org/10.1016/j.scitotenv.2020.140134

Chen L, Tian L, Xie J et al (2020) One-step solid state synthesis of facet-dependent contact TiO2 hollow nanocubes and reduced graphene oxide hybrids with 3D/2D heterojunctions for enhanced visible photocatalytic activity. Appl Surf Sci 504:144353. https://doi.org/10.1016/j.apsusc.2019.144353

Chen L, Tian L, Zhao X et al (2020) SPR effect of Au nanoparticles on the visible photocatalytic RhB degradation and NO oxidation over TiO2 hollow nanoboxes. Arab J Chem 13:4404–4416. https://doi.org/10.1016/j.arabjc.2019.08.011

Colmenares JC, Varma RS, Nair V (2017) Selective photocatalysis of lignin-inspired chemicals by integrating hybrid nanocatalysis in microfluidic reactors. Chem Soc Rev 46:6675–6686. https://doi.org/10.1039/c7cs00257b

Dai C, Tian X, Nie Y et al (2018) Surface facet of CuFeO2 nanocatalyst: a key parameter for H2O2 activation in Fenton-like reaction and organic pollutant degradation. Environ Sci Technol 52:6518–6525. https://doi.org/10.1021/acs.est.8b01448

Dai Q, Yuan B, Guo M et al (2020) A novel nano-fibriform C- modified niobium pentoxide by using cellulose templates with highly visible-light photocatalytic performance. Ceram Int 46:13210–13218. https://doi.org/10.1016/j.ceramint.2020.02.096

de Luna MDG, Briones RM, Su C-C, Lu M-C (2013) Kinetics of acetaminophen degradation by Fenton oxidation in a fluidized-bed reactor. Chemosphere 90:1444–1448. https://doi.org/10.1016/j.chemosphere.2012.09.003

Ding Y, Yan Y, Wang H et al (2018) Preparation of hollow Cu and CuOx, microspheres with a hierarchical structure for heterogeneous catalysis. ACS Appl Mater Interfaces 10:41793–41801. https://doi.org/10.1021/acsami.8b16246

Dong Y, Tao F, Wang L et al (2020) One-pot preparation of hierarchical Cu2O hollow spheres for improved visible-light photocatalytic properties. RSC Adv 10:22387–22396. https://doi.org/10.1039/d0ra02460k

Esmaeili S, Zanjanchi MA, Golmojdeh H, Shariati S (2020) Synthesis, characterization and photocatalytic studies of MCM-41 mesoporous silica core-shells doped with selenium oxide and lanthanum ions. Microporous Mesoporous Mat 292:109714. https://doi.org/10.1016/j.micromeso.2019.109714

Gao C, Wang J, Xu H, Xiong Y (2017) Coordination chemistry in the design of heterogeneous photocatalysts. Chem Soc Rev 46:2799–2823. https://doi.org/10.1039/c6cs00727a

Ghafoori S, Mehrvar M, Chan PK (2014) Photoreactor scale-up for degradation of aqueous poly(vinyl alcohol) using UV/H2O2 process. Chem Eng J 245:133–142. https://doi.org/10.1016/j.cej.2014.01.055

Gholizadeh EM, Prasad SKK, Teh ZL, et al (2020) Photochemical upconversion of near-infrared light from below the silicon bandgap. Nat Photonics 14:585-+. https://doi.org/10.1038/s41566-020-0664-3

Gui W, Lin J, Liang Y et al (2019) A two-step strategy for high-efficiency fluorescent dye removal from wastewater. NPJ Clean Water 2:16. https://doi.org/10.1038/s41545-019-0041-2

Hodges BC, Cates EL, Kim J-H (2018) Challenges and prospects of advanced oxidation water treatment processes using catalytic nanomaterials. Nat Nanotechnol 13:642–650. https://doi.org/10.1038/s41565-018-0216-x

Huang Z, Liu J, Huang L et al (2020) One-step synthesis of dandelion-like lanthanum titanate nanostructures for enhanced photocatalytic performance. NPG Asia Mater 12:11. https://doi.org/10.1038/s41427-019-0194-y

Islam MR, Saiduzzaman M, Nishat SS et al (2021) Synthesis, characterization and visible light-responsive photocatalysis properties of Ce doped CuO nanoparticles: a combined experimental and DFT plus U study. Colloid Surf A-Physicochem Eng Asp 617:126386. https://doi.org/10.1016/j.colsurfa.2021.126386

Kadi MW, Mohamed RM, Ismail AA (2020) Uniform dispersion of CuO nanoparticles on mesoporous TiO2 networks promotes visible light photocatalysis. Ceram Int 46:8819–8826. https://doi.org/10.1016/j.ceramint.2019.12.124

Kamat PV (2017) Semiconductor surface chemistry as holy grail in photocatalysis and photovoltaics. Accounts Chem Res 50:527–531. https://doi.org/10.1021/acs.accounts.6b00528

Kanjana N, Maiaugree W, Poolcharuansin P, Laokul P (2020) Size controllable synthesis and photocatalytic performance of mesoporous TiO2 hollow spheres. J Mater Sci Technol 48:105–113. https://doi.org/10.1016/j.jmst.2020.03.013

Kinetics, Thermodynamics, and modeling of amido black dye photodegradation in water using Co/TiO2 nanoparticles - Ali - 2018 - Photochemistry and Photobiology - Wiley Online Library. https://webvpn1.jiangnan.edu.cn/https/77726476706e69737468656265737421fff94d95293564597c1a88be811b343cb55cc5e3193677/doi/https://doi.org/10.1111/php.12937. Accessed 24 Mar 2022

Kisch H (2017) Semiconductor photocatalysis for chemoselective radical coupling reactions. Accounts Chem Res 50:1002–1010. https://doi.org/10.1021/acs.accounts.7b00023

Li X, Huang R, Hu Y et al (2012) A templated method to Bi2WO6 Hollow microspheres and their conversion to double-shell bi2o3/bi2wo6 hollow microspheres with improved photocatalytic performance. Inorg Chem 51:6245–6250. https://doi.org/10.1021/ic300454q

Li A, Zhu W, Li C et al (2019) Rational design of yolk-shell nanostructures for photocatalysis. Chem Soc Rev 48:1874–1907. https://doi.org/10.1039/c8cs00711j

Li Y, Peng Y-K, Hu L et al (2019) Photocatalytic water splitting by N-TiO2 on MgO (111) with exceptional quantum efficiencies at elevated temperatures. Nat Commun 10:4421. https://doi.org/10.1038/s41467-019-12385-1

Li M, Gao X, Liu H et al (2020) Preparation of heterogeneous Fenton catalyst gamma-Cu-Ce-Al2O3 and the evaluation on degradation of phenol. Environ Sci Pollut Res 27:21476–21486. https://doi.org/10.1007/s11356-020-08648-w

Li Y, Shen Q, Guan R et al (2020) A C@TiO2 yolk-shell heterostructure for synchronous photothermal-photocatalytic degradation of organic pollutants. J Mater Chem C 8:1025–1040. https://doi.org/10.1039/c9tc05504e

Li L, Hu C, Zhang L, Shi B (2021) More octahedral Cu+ and surface acid sites in uniformly porous Cu-Al2O3 for enhanced Fenton catalytic performances. J Hazard Mater 406:124739. https://doi.org/10.1016/j.jhazmat.2020.124739

Li X, Min X, Hu X et al (2021) In-situ synthesis of highly dispersed Cu-CuxO nanoparticles on porous carbon for the enhanced persulfate activation for phenol degradation. Sep Purif Technol 276:119260. https://doi.org/10.1016/j.seppur.2021.119260

Liang Q, Gao W, Liu C et al (2020) A novel 2D/1D core-shell heterostructures coupling MOF-derived iron oxides with ZnIn2S4 for enhanced photocatalytic activity. J Hazard Mater 392:122500. https://doi.org/10.1016/j.jhazmat.2020.122500

Liang Y, Chen Y, Lin L et al (2020) An in situ ion exchange grown visible-light-driven Z-scheme AgVO3/AgI graphene microtube for enhanced photocatalytic performance. New J Chem 44:1579–1587. https://doi.org/10.1039/c9nj05376j

Liang Q, Liu X, Wang J et al (2021) In-situ self-assembly construction of hollow tubular g-C3N4 isotype heterojunction for enhanced visible-light photocatalysis: experiments and theories. J Hazard Mater 401:123355. https://doi.org/10.1016/j.jhazmat.2020.123355

Muthukrishnaraj A, Kalaivani SS, Manikandan A et al (2020) Sonochemical synthesis and visible light induced photocatalytic property of reduced graphene oxide@ZnO hexagonal hollow rod nanocomposite. J Alloy Compd 836:155377. https://doi.org/10.1016/j.jallcom.2020.155377

(2021) Preparation and characterization of oxidized graphene for actinides and rare earth elements removal in nitric acid solutions from nuclear wastes. Journal of Molecular Liquids 335:116260. https://doi.org/10.1016/j.molliq.2021.116260

Raees A, Jamal MA, Ahmed I et al (2021) Synthesis and characterization of CeO2/CuO nanocomposites for photocatalytic degradation of methylene blue in visible light. Coatings 11:305. https://doi.org/10.3390/coatings11030305

Ren X, Wang J, Yu J et al (2021) Waste valorization: transforming the fishbone biowaste into biochar as an efficient persulfate catalyst for degradation of organic pollutant. J Clean Prod 291:125225. https://doi.org/10.1016/j.jclepro.2020.125225

Shang S, Jiao X, Chen D (2012) Template-free fabrication of TiO2 Hollow spheres and their photocatalytic properties. ACS Appl Mater Interfaces 4:860–865. https://doi.org/10.1021/am201535u

Shuang Z, Gza B, Xin WC, Mga B (2020) Enhanced catalytic degradation of polyvinyl alcohol from aqueous solutions by novel synthesis of MnCoO 3 @γ-Al 2 O 3 nanocomposites: performance, degradation intermediates and mechanism. J Mol Liq 323:114569. https://doi.org/10.1016/j.molliq.2020.114569

Smith JD, Jamhawi AM, Jasinski JB et al (2019) Organopolymer with dual chromophores and fast charge-transfer properties for sustainable photocatalysis. Nat Commun 10:1837. https://doi.org/10.1038/s41467-019-09316-5

(2018) Stereoselective uptake and degradation of (±)-o,p-DDD pesticide stereomers in water-sediment system. Chirality 30:1088–1095. https://doi.org/10.1002/chir.22989

Strieth-Kalthoff F, James MJ, Teders M et al (2018) Energy transfer catalysis mediated by visible light: principles, applications, directions. Chem Soc Rev 47:7190–7202. https://doi.org/10.1039/c8cs00054a

Su Z, Li J, Zhang D et al (2019) Novel flexible Fenton-like catalyst: unique CuO nanowires arrays on copper mesh with high efficiency across a wide pH range. Sci Total Environ 647:587–596. https://doi.org/10.1016/j.scitotenv.2018.08.022

Wang J, Xiong Z, Zheng J et al (2018) Light-driven micro/nanomotor for promising biomedical tools: principle, challenge, and prospect. Accounts Chem Res 51:1957–1965. https://doi.org/10.1021/acs.accounts.8b00254

Wang H, Tang Q, Chen Z et al (2020) Recent advances on silica-based nanostructures in photocatalysis. Sci China-Mater 63:2189–2205. https://doi.org/10.1007/s40843-020-1381-y

Wang H, Wang H, Wang Z et al (2020) Covalent organic framework photocatalysts: structures and applications. Chem Soc Rev 49:4135–4165. https://doi.org/10.1039/d0cs00278j

Wang J, Li B, Li Y et al (2021) Easily regenerated CuO/gamma-Al2O3 for persulfate-based catalytic oxidation: insights into the deactivation and regeneration mechanism. ACS Appl Mater Interfaces 13:2630–2641. https://doi.org/10.1021/acsami.0c19013

Xiao M, Wang Z, Lyu M et al (2019) Hollow Nanostructures for photocatalysis: advantages and challenges. Adv Mater 31:1801369. https://doi.org/10.1002/adma.201801369

Yang X, Wang D (2018) Photocatalysis: from fundamental principles to materials and applications. ACS Appl Energ Mater 1:6657–6693. https://doi.org/10.1021/acsaem.8b01345

Zhang H, Duan S, Radjenovic PM et al (2020) Core-shell nanostructure-enhanced raman spectroscopy for surface catalysis. Accounts Chem Res 53:729–739. https://doi.org/10.1021/acs.accounts.9b00545

Zhao X, Su Y, Qi X, Han X (2017) A facile method to prepare novel Ag2O/Ag2CO3 three-dimensional hollow hierarchical structures and their water purification function. ACS Sustain Chem Eng 5:6148–6158. https://doi.org/10.1021/acssuschemeng.7b01040

Zhao H, Cui S, Li G et al (2020) 1T-and 2H-mixed phase MoS2 nanosheets coated on hollow mesoporous TiO2 nanospheres with enhanced photocatalytic activity. J Colloid Interface Sci 567:10–17. https://doi.org/10.1016/j.jcis.2020.01.100

Zhou Z, Zhang Y, Shen Y et al (2018) Molecular engineering of polymeric carbon nitride: advancing applications from photocatalysis to biosensing and more. Chem Soc Rev 47:2298–2321. https://doi.org/10.1039/c7cs00840f

Zhou Y, Lu J, Liu Q et al (2020) A novel hollow-sphere cyclodextrin nanoreactor for the enhanced removal of bisphenol A under visible irradiation. J Hazard Mater 384:121267. https://doi.org/10.1016/j.jhazmat.2019.121267